Josephson coupled Ising pairing induced in suspended MoS2 bilayers by double-side ionic gating

Zheliuk, O.; Lu, J. M.; Chen, Q. H.; El Yumin, A. A.; Golightly, S.; Ye, J. T.

Published in:
Nature Nanotechnology

DOI:
10.1038/s41565-019-0564-1

Publication date:
2019

nature nanotechnology

ARTICLES

https://doi.org/10.1038/s41565-019-0564-1

Corrected: Publisher Correction

Josephson coupled Ising pairing induced in suspended MoS_2 bilayers by double-side ionic gating

O. Zheliuk[1], J. M. Lu[1,2,3], Q. H. Chen[1], A. A. El Yumin[1], S. Golightly[1] and J. T. Ye[1]*

Superconductivity in monolayer transition metal dichalcogenides is characterized by Ising-type pairing induced via a strong Zeeman-type spin–orbit coupling. When two transition metal dichalcogenides layers are coupled, more exotic superconducting phases emerge, which depend on the ratio of Ising-type protection and interlayer coupling strength. Here, we induce superconductivity in suspended MoS_2 bilayers and unveil a coupled superconducting state with strong Ising-type spin–orbit coupling. Gating the bilayer symmetrically from both sides by ionic liquid gating varies the interlayer interaction and accesses electronic states with broken local inversion symmetry while maintaining the global inversion symmetry. We observe a strong suppression of the Ising protection that evidences a coupled superconducting state. The symmetric gating scheme not only induces superconductivity in both atomic sheets but also controls the Josephson coupling between the layers, which gives rise to a dimensional crossover in the bilayer.

In superconducting monolayer transition metal dichalcogenides (TMD), the spins of a Cooper pair are strongly aligned by a Zeeman-type spin–orbit coupling (SOC) (β_{SO}) in the vicinity of K and K' points of the conduction and valence bands of the hexagonal Brillouin zone forming so-called Ising pairing[1–4]. The strong out-of-plane spin alignment, which alternates at the K and K' points, makes this family of superconductors highly robust against an in-plane magnetic field. The resilience of pairing can be parameterized by the degree of violation of the Pauli limiting field $B_p = 1.86$ [T/K] T_{c0}, which is estimated for a Bardeen–Cooper–Schrieffer-type superconductor with a transition temperature T_{c0}. For typical Ising superconductivity observed in TMD monolayers, the ratio between upper critical field B_{c2} and B_p ranges from around 5–6 in MoS_2 ($\beta_{SO} = 6.2$ meV)[1] and $NbSe_2$ (~76 meV)[2], to ~9 in TaS_2 (~122 meV)[5] and more than 40 in monolayer WS_2 (30 meV)[4]. However, when two or more layers are stacked together, the spin configuration of superconductivity in many TMDs can be influenced by interlayer coupling to form a coupled state.

On the basis of the monolayer superconductivity configured by SOC, more exotic pairing schemes can be prepared by coupling two identical layers, for which two types of systems have been proposed theoretically[6–8]. One type requires the coupling between two superconducting layers with Rashba-type SOC[6], which has been studied in the superlattices of $CeCoIn_5$ (ref. [9]). Whereas the other type is based on Zeeman-type SOC involving two Ising pairings with opposite spin configurations coupled through Josephson interaction. The coupled state, having a finite centre-of-mass momentum q, is predicted as a Fulde–Ferrell–Larkin–Ovchinnikov (FFLO) state[7,8]. The realization of such a coupled system is not only of theoretical interest. Technically, the ability to control the Ising state at a specific location can build superconducting junctions formed by adjacent regions having a similar T_{c0} but drastically different B_{c2}, which is demonstrated in Section 4 of the Supplementary Information (Supplementary Fig. 5b).

As the strong SOC is an intrinsic property of many TMDs of 2H phase, the Ising pairing thus configured by the SOC is inherently protected against the external in-plane magnetic field. On the other hand, the interlayer interaction can mix the spin configurations of the individual layers. Hence, the Ising protection in the coupled state is expected to be substantially weakened. At the same time, the vector potential of the magnetic field can enter the kinetic energy of electron causing orbital effect, which enhances with the increase of layer numbers. This weakens the superconducting state due to enhanced orbital depairing in the in-plane B field[2,5,10]. Therefore, the superconducting bilayer 2H-type $NbSe_2$ and TaS_2 (refs. [2,5]) are regarded as the candidates for observing the coupled states. However, the interlayer coupling in both bilayers can only cause a small decrease of B_{c2} compared with that of a monolayer, which is not consistent with the gross reduction predicted as the signature of effective coupling, indicating a coupled state is yet to be prepared. For the Ising pairing in the valence band of 2H-type TaS_2 and $NbSe_2$, the relevant pairing suppression mechanism such as Rashba-type SOC and interlayer interaction are much smaller than the intrinsic Ising-type SOC (Supplementary Table 4). For example, a typical ratio between interlayer coupling t and β_{SO} in bilayer TaS_2 and $NbSe_2$ are 0.31 and 0.056, respectively[5]. Therefore, to reach the coupled state that can significantly influence the Ising protection, weaker intrinsic SOC found in the conduction band of MoS_2 stands out as the natural choice.

Phase diagram of suspended bilayer MoS_2

The bilayer 2H-MoS_2 exhibits global inversion symmetry (point P marked between two layers in Fig. 1a) while maintaining the broken inversion symmetry locally within the individual layers[11]. Inducing carrier in the lower-lying electron pockets (Fig. 1b), symmetric superconducting states in both top and bottom layers can be prepared by applying strong electric fields E_{LG} from ionic liquid gating as shown schematically in Fig. 1c. An in-plane magnetic

[1]Device Physics of Complex Materials, Zernike Institute for Advanced Materials, University of Groningen, Groningen, the Netherlands. [2]High Field Magnet Laboratory, Radboud University, Nijmegen, the Netherlands. [3]State Key Laboratory for Mesoscopic Physics, School of Physics, Peking University, Beijing, China. *e-mail: j.ye@rug.nl

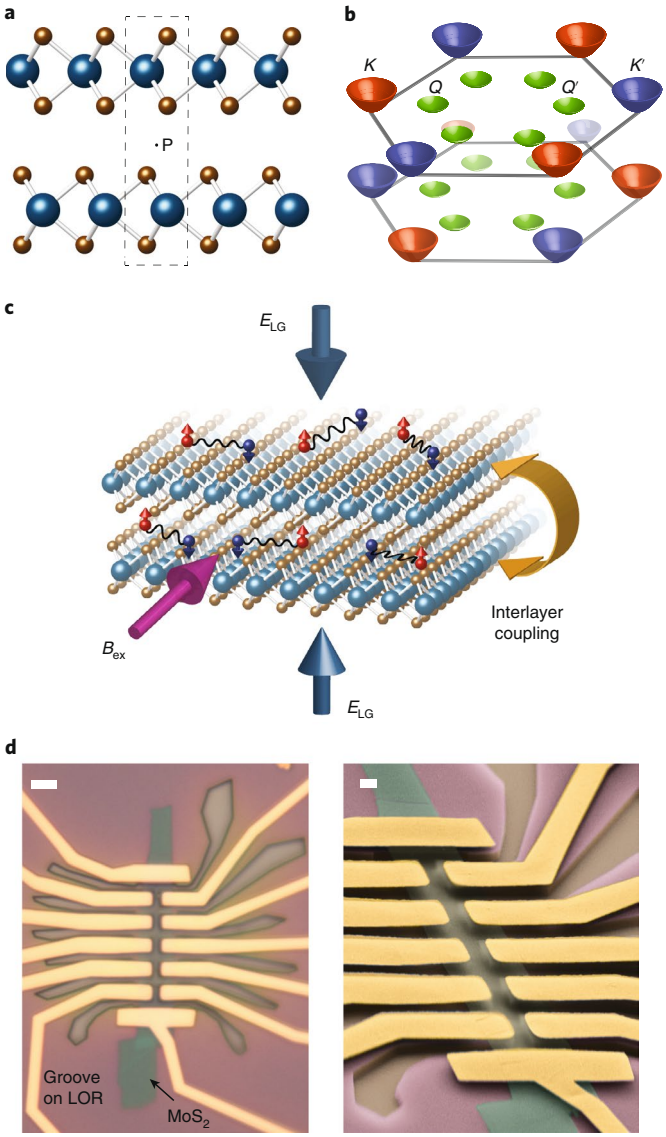

Fig. 1 | Crystal and device structure of suspended MoS_2 bilayer. **a**, Side view of the crystal structure of a bilayer 2H-MoS_2, where the Mo and S atoms are coloured in blue and brown, respectively. A unit cell is enclosed by the dashed rectangle, where the inversion symmetry point P is located between two neighbouring layers. **b**, The hexagonal Brillouin zone of a bilayer MoS_2 and the electron doping near the conduction band edge. The electrons of the top and bottom layer near the one *K*/*K*′ point shows the opposite spin configuration. The up (red)/down (blue) spin at *K*/*K*′ point is switched between layers. **c**, Schematic configuration of the double-side gating on a bilayer MoS_2. The superconducting state is induced by the strong electric field E_{LG} (blue arrows) generated by accumulating ions on both top and bottom layers. The effect of interlayer interaction (orange arrow) on Ising protection is probed by the external in-plane magnetic field B_{ex} (purple arrow). **d**, Optical micrograph (left) and false-colour scanning electron microscope image (right) of a typical Hall-bar device of a bilayer MoS_2 suspended over trenches on LOR before being immersed into the ionic liquid. Scale bars: left, 4 μm and right, 1 μm.

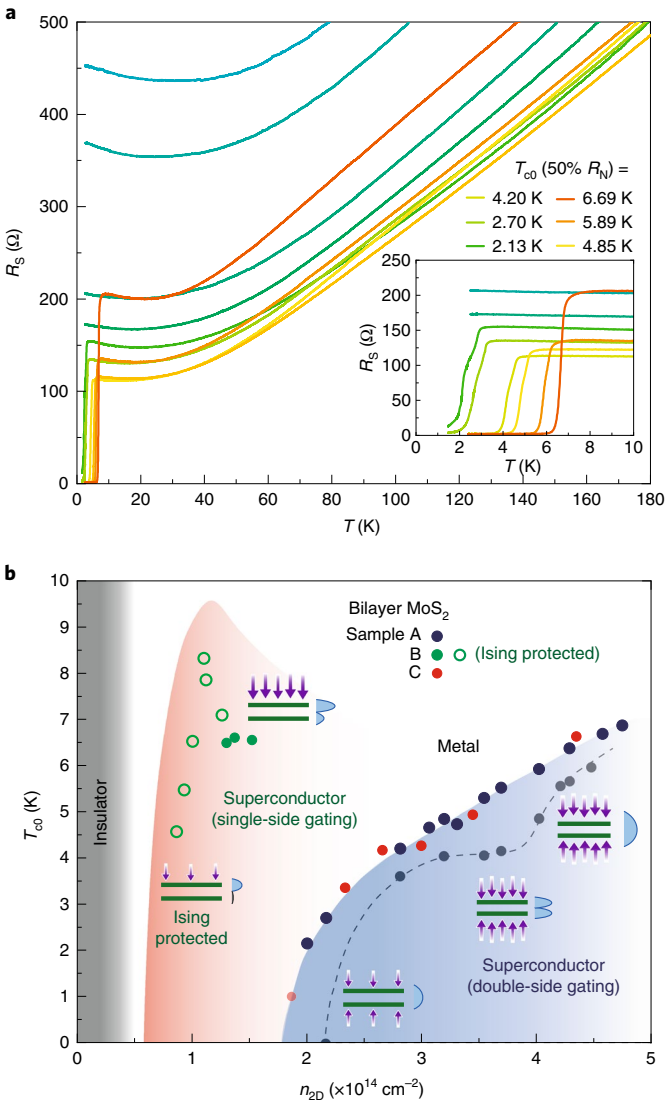

Fig. 2 | Superconducting phase diagram. a, The temperature dependence of sheet resistance R_S of Sample A. A set of states having different T_{c0} values (labelled by different colours) was accessed by ionic gating. The inset shows the expanded temperature region close to the superconducting transitions. **b**, Superconducting phase diagram of the single- (green, Sample B) and double-side (blue and red, Sample A and C) gated bilayer devices with the onsets close to $n_{2D} = 0.6 \times 10^{14}$ and 1.8×10^{14} cm^{-2}, respectively. The red shaded region is reproduced from ref. [14]. The critical temperature T_{c0} is defined as 50% of the normal resistance R_N. The dashed line is a guide for the eye for the crossover temperature T^* extracted from the upper critical field measurements for Samples A (Fig. 3a) and C (Supplementary Fig. 5).

field B_{ex} can then be applied to probe the robustness of the Ising pairing. This scheme is implemented by suspending a bilayer MoS_2 flake on an undercut of around 0.8–1 μm in width[12,13]. As shown in Fig. 1d, without having extended exposure, the suspended bilayer remains flat under electron microscopy. At room temperature, the highly fluidic ionic liquid can permeate through the undercut and contact both top and bottom surfaces. Hence, carriers can be induced symmetrically by E_{LG} on both sides of the flake by applying a single gate bias.

Similar to the single-side gated multilayers[14], applying the gate bias on the suspended bilayer induces superconductivity as shown in Fig. 2a. The transition temperature, T_{c0}, measured at a magnetic field $B = 0$, varies as a function of two-dimensional carrier density n_{2D}, which was measured at 10 K by the Hall effect (Supplementary Fig. 6). As shown in the phase diagram (Fig. 2b), the superconductivity emerges near $n_{2D} = 1.8 \times 10^{14}$ cm^{-2}, which is significantly higher than that observed in single-side gated devices

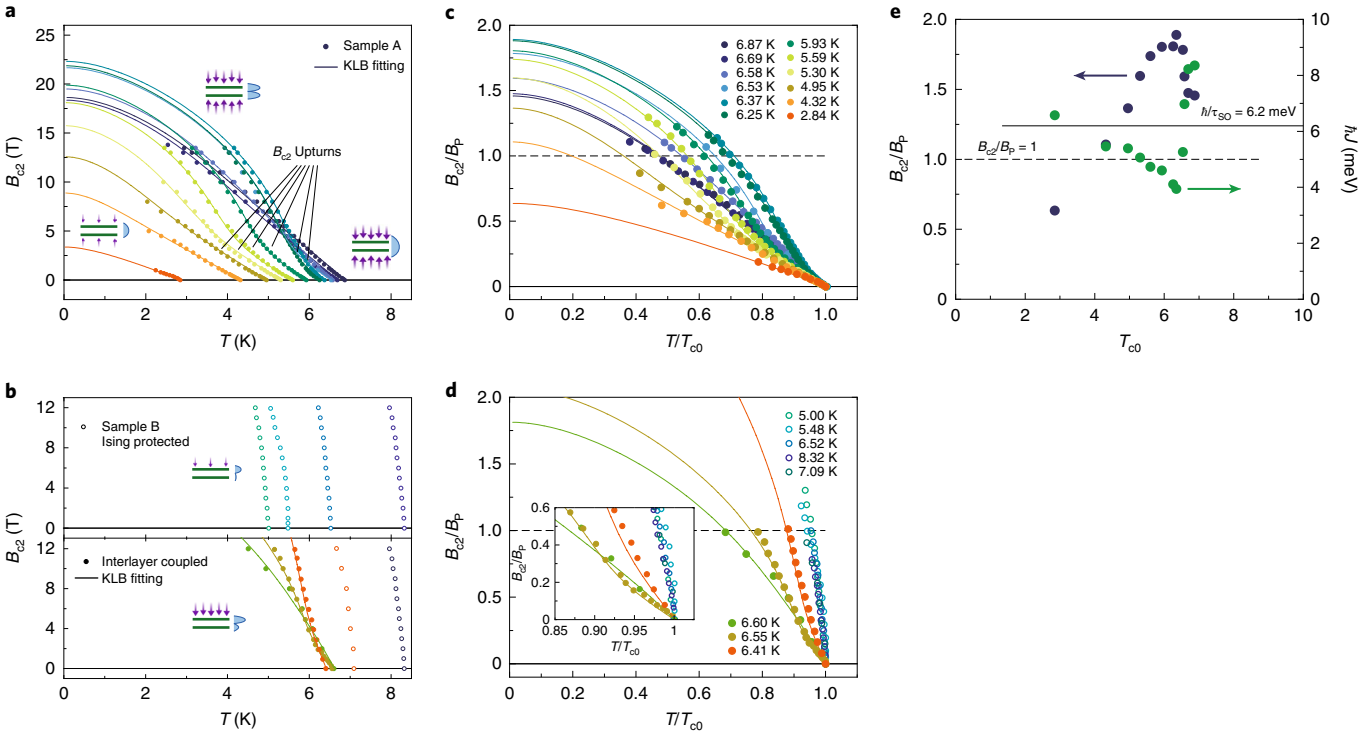

Fig. 3 | Upper critical field measurements for single- and double-side gating on a bilayer MoS_2. a, The temperature dependence of in-plane upper critical field B_{c2} of Sample A for different T_{c0} states. Three schematic profiles of carrier distribution in the bilayer after double-side gating are plotted for the states induced by weak (left), intermediate (middle) and strong (right) gating. The solid curves correspond to the KLB fitting where the increase of the slope of $B_{c2}-T$ dependences close to T_{c0} is marked by the B_{c2} upturns. **b**, The in-plane B_{c2} of Sample B, gated from a single side, measured at states with different T_{c0}. The schematic doping profiles in upper and lower panels correspond to the cases of weak and strong gating, respectively. The suppression of B_{c2} appears when T_{c0} passes the superconducting dome peak (corresponding to the filled green circles in Fig. 2b). The open and filled circles correspond to B_{c2} with Ising protected and bilayer coupled states, respectively. **c**, The B_{c2}/B_P is plotted as a function of normalized temperature T/T_{c0} for all states shown in **a**. The dashed line indicates the Pauli limit $B_{c2}/B_P=1$. **d**, The B_{c2}/B_P versus T/T_{c0} diagram for all states in **b**. The symbols and colours are matched with the data shown in **b**. The KLB fitting is enlarged in the inset for the upturn of the curvature near the T_{c0}. **e**, As a function of different superconducting states of Sample A with different T_{c0} values, the left and right axes show $B_{c2}(0\,K)/B_P$ and Josephson coupling energy $\hbar J$, respectively. Both $B_{c2}(T=0\,K)$ and $\hbar J$ are extracted from KLB fitting of Sample A.

$(0.6\times10^{14}\,cm^{-2})$[14]. If gated only from the topside, the strong electric field confines carriers to the topmost layer breaking inversion symmetry and populating electrons in the K and K' pockets, mimicking the band structure of a freestanding monolayer[15,16]. Whereas gating from both sides of a bilayer MoS_2 preserves the global inversion symmetry and induces carriers also in Q pockets in addition to the K pockets[17], accommodating more carriers than simply doubling that required for the single-side gating. In double-side gated Sample A (Fig. 2b), the T_{c0} increases monotonically with the increase of n_{2D} reaching highest $T_{c0}=6.87\,K$ at $n_{2D}=4.75\times10^{14}\,cm^{-2}$, the highest n_{2D} accessed in this device. Applying strong gating to a monolayer TMD can cause a decrease of T_{c0}, which eventually enters a highly resistive re-entrance state[4,18]. In contrast, no clear T_{c0} saturation was observed even at the maximum gating in the bilayer. This is consistent with the larger density of states from the additional Q/Q' pockets, which also enhances the screening. Although metallic transport and superconducting state maintains at the maximum applied ionic gating, the normal resistance R_N, measured just above T_{c0}, increases by ~100 Ω for states from $T_{c0}=4.2$ to 6.8 K. The systematic increase of the sheet resistance R_S indicates the increasing contribution from the localization effect (Fig. 2b), a tendency approaching the re-entrant insulating state towards the dome peak[4].

In-plane upper critical field of the coupled Ising state

The resilience of the induced superconducting states (Fig. 2a) against in-plane magnetic field B_{ex} was then examined. As shown in Fig. 3a, we plot the temperature dependence of B_{c2} of Sample A for superconducting states with different induced carrier density n_{2D} and critical temperature T_{c0}. The overall Ising protection is strongly suppressed in contrast with the single-side gated MoS_2, where the B_{c2}/B_P of ~6 was typically observed[1]. The B_{c2} of double-side gated devices shows a strong and non-monotonic change with T_{c0} (Fig. 3a). The B_{c2} values for the states with $T_{c0}<5\,K$ are comparable or lower than the B_P. For the states with $T_{c0}>5\,K$, the temperature dependence of B_{c2} shows a clear feature of a 2D to bulk three-dimensional crossover at T^* close T_{c0}, which was observed previously in layered bulk superconductors with strong 2D anysotropy[19]. At $T<T^*$, the out-of-plane coherence length $\xi_\perp$ becomes smaller than the interlayer spacing, which defines the condition of establishing a Josephson vortex between the layers. As a typical example, the bulk 2H-TaS_2 is an anisotropic three-dimensional superconductor with a weak anisotropy ratio $\gamma=\frac{B_{c2}^{\parallel}}{B_{c2}^{\perp}}\approx6$. By intercalating organic molecule spacers[19], the expanded layers reduce Josephson coupling, resulting in a larger anisotropy ratio $\gamma=\frac{B_{c2}^{\parallel}}{B_{c2}^{\perp}}\approx60$. The Ising pairing in a monolayer TaS_2 with the extrapolated B_{c2}/B_P ratio of 9 at zero temperature reduces slightly to ~6 in a bilayer[20] case. The further reduction of B_{c2}/B_P is even smaller when the layer number increases from 2 to 5 (ref. [5]). Compared with the static value for a given thickness, the B_{c2} shown in Fig. 3a,c can be electrostatically tuned. Compare with the B_{c2}/B_P of ~6 found in bilayer 2H-TaS_2, here the B_{c2} can be suppressed well below B_P due to the comparable energy scales of Josephson coupling over spin–orbit interaction: $\hbar J/\beta_{SO}$. The gate controllable $\hbar J$ then

enables an effective competition. Therefore, Ising protection can be effectively tuned and reduced even to $B_{c2} < B_p$.

To understand the upturn curvature of B_{c2} near T_{c0} for the states with T_{c0} between 5 and 6.6 K, we applied the microscopic Klemm–Luther–Beasley (KLB) theory[21,22] to fit the temperature dependence of B_{c2} (solid lines in Fig. 3a). The representative parameters extracted from KLB fitting such as the intrinsic spin–orbit interaction and the Josephson coupling between the layers are listed in Supplementary Table 1 and Supplementary Fig. 3. Here, the phase diagram is shaped by the interplay between spin–orbit interaction and Josephson coupling $\hbar J$. The states with $T_{c0} < 5$ K and $T_{c0} > 6.6$ K show a nearly linear temperature dependence of B_{c2} close T_{c0}. This behaviour can be assigned to three-dimensional-like states due to strong Josephson coupling. The $\hbar J$ is $>0.85\beta_{so}$, where orbital pair-breaking effect dominates. The states with T_{c0} between 5 and 6.6 K are characterized by the Josephson coupled three-dimensional state and decoupled 2D state above and below T^*, respectively, causing an upturn of the temperature dependence of B_{c2} at T^*. The correlation between this upturn feature and formation of Josephson coupling between two adjacent layers was carefully analysed by KLB theory in bulk doped TaS_2 (ref. [19]). Our observation of the clear upturn of the curvature, for states with $\frac{\hbar J}{\beta_{SO}} = 0.66-0.85$ and T_{c0} between 5 and 6.6 K, shows clear evidence that Josephson vortices were established in a bilayer. The presence of Josephson vortex is a prerequisite to realize FFLO state in present bilayer system[7,8].

To confirm the strong suppression of B_{c2} and especially to remove the concern about the flatness of the flake after suspension, a control experiment was performed on a single-side gated device of bilayer MoS_2 prepared on flat SiO_2/Si substrate (Fig. 3b). In spite of the flat surface shown in Fig. 1d, small curvature is still possible and is difficult to characterize after immersing the suspended bilayer into the ionic liquid, which might couple to the in-plane field causing the observed phenomena. In sharp contrast to the suppression observed in double-side gating (Fig. 3a,b is plotted with the same scales in B and T), a strongly protected Ising state was observed close to the onset of superconducting dome 0.6×10^{14} cm^{-2}, which is consistent with the dominant contribution from the topmost layer (phase diagram in Fig. 2b) and previous observations in single-side gated multilayers, where the stronger protection was found in the states with lower T_{c0} (ref. [1]). Inducing higher carrier concentration above the onset, the T_{c0} follows the previously established phase diagram (the red shaded region from ref. [14] in Fig. 2b) and reaches the dome peak. For the states with T_{c0} on the left side of the dome peak, the temperature dependence of B_{c2} remains steep as shown in the upper panel of Fig. 3b. For the states having T_{c0} on the right side of the dome peak, carriers are increasingly doped to the second layer by the electric field penetrated from the top monolayer due to the intrinsically weak screening effect of a 2D system[4]. Therefore, superconductivity is increasingly shared by both MoS_2 layers. The variation of B_{c2} in this process can be described by the changing $\hbar J$ from zero (data with open circles, starting with lowest T_{c0} in the upper panel of Fig. 3b) to a finite value (data shown in filled circles in the lower panel of Fig. 3b) mimicking the enhancement of Josephson interaction. As a result, for states in both layers accessed by strong gating (gold and red curves in Fig. 3b), a clear upturn of the curvature region characteristic for the dimensional crossover is also observed close to the T_{c0}. Although the Ising protection is also reduced by $\hbar J$, the degree of reduction of B_{c2}/B_P is smaller than that observed in double-side gated samples (Fig. 3a), where the coupling is stronger between two identically doped superconducting layers.

As shown in Fig. 3a, the B_{c2}/B_P ratio does not follow the change of T_{c0} monotonically. Especially, for the states with $T_{c0} > 6$ K, the upturn of the curvature becomes less prominent, which is concomitant with the decrease of B_{c2}/B_P. This anomalous dependence can be clearly seen in Fig. 3e, where the B_{c2}/B_P ratio at zero temperature and Josephson coupling $\hbar J$ were extracted from KLB fitting for superconducting

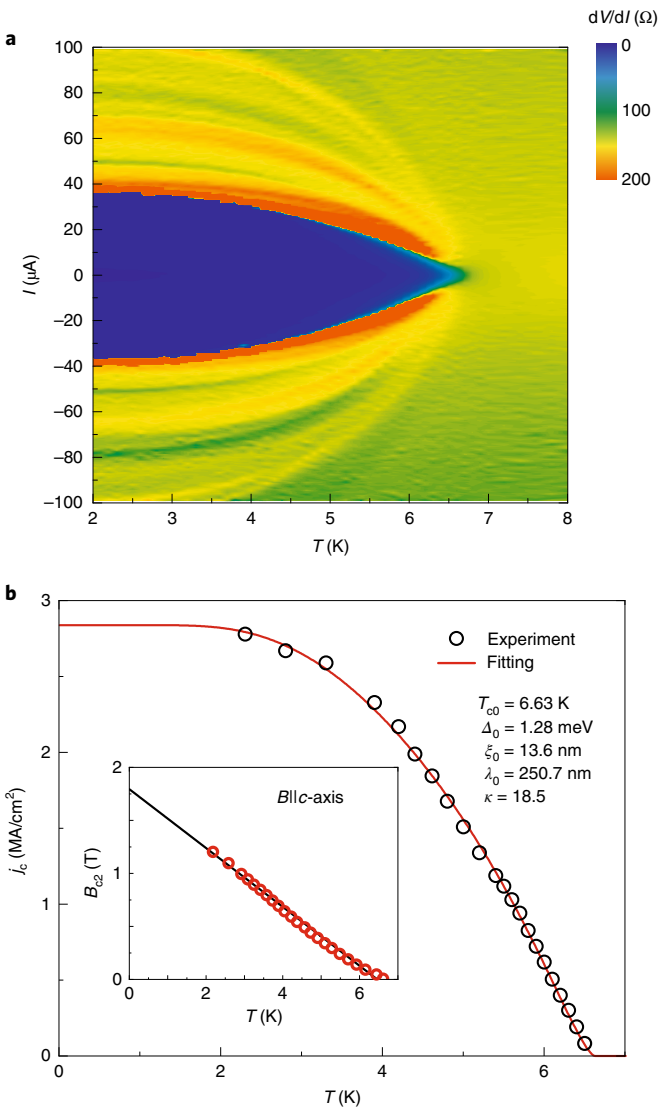

Fig. 4 | The *I*–*V* mapping of the double-side gated bilayer MoS_2. **a**, The temperature dependence of differential resistance d*V*/d*I* for the superconducting state with $T_{c0} = 6.63$ K. **b**, The temperature dependence of the critical current density j_c (black circle) extracted from **a** and the fitting using a single-band self-field critical current model (red line). The inset shows the temperature dependence of the out-of-plane (B||c-axis) critical field (red circles) of the same state shown in **a**. The zero-temperature coherence length ξ_0 obtained from Ginzburg–Landau fitting (black line) was used to fit the $j_c(T)$ curve. Here, the κ and λ_0 are the Ginzburg–Landau parameter and London penetration depth, respectively.

states of different T_{c0} values. By assuming constant spin–orbit protection, the ratio of B_{c2}/B_P is mainly affected by the gate tuneable $\hbar J$. Details of the fitting can be found in Section 2 of the Supplementary Information and Supplementary Fig. 3. As shown in Fig. 3e, the anti-correlation between B_{c2}/B_P and $\hbar J$ is observed for the entire phase diagram for each accessed state with different T_{c0} values. The $\hbar J$ decreases gradually with the increase of T_{c0} reaching the minimum of 3.95 meV for the state with $T_{c0} = 6.35$ K. This monotonic decrease is stopped by an abrupt increase up to 8.35 meV within a narrow range of T_{c0} from 6.35 to 6.69 K, which can be reversibly accessed by gating. The Josephson coupling is modified mostly by the applied electric field E, which changes the doping profile of induced carriers. For the states with $T_{c0} \leq 4$ K, the induced carrier is centrosymmetric

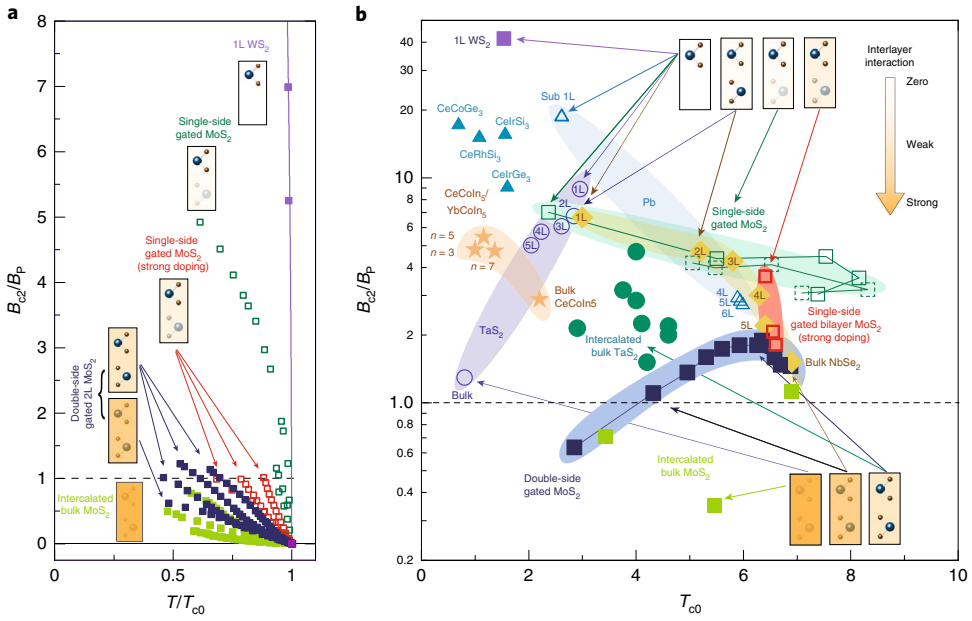

Fig. 5 | The interplay between SOC and interlayer interaction in superconductors with large in-plane B_{c2}. a, The systematic variation of the B_{c2} in 2H-MoS_2 (same legend as in **b**) with the change of interlayer coupling. The schematics of the competing influence of SOC and strength of the interlayer interaction is pictorially shown as the shade changes from light to dark orange, where darker shade corresponds to stronger interaction. **b**, The enhancement of B_{c2}/B_P as a function of T_{c0} for typical non-centrosymmetric and centrosymmetric superconductors with broken local inversion symmetry, which includes the pristine, intercalated and gate-induced superconductivity in TMDs. The widely used criteria of 50% of R_N was chosen to determine T_{c0}. And the B_{c2} at the limit of zero temperature was determined from KLB fitting. The data points belonging to the same superconductor are shaded as a guide for the eye. The uneven carrier distribution in single-side gated bilayer MoS_2 illustrates the reduced Ising protection having partial shading. In MoS_2 bilayers, the broken inversion symmetry in single-side gated bilayer by relatively low electric field gives rise to strong Ising protection of ~$4B_P$ (green squares), which can be continuously suppressed to ~$1.6B_P$ when sufficient amount of carriers are induced in the second layer, hence partially restoring the inversion symmetry (red square). By adding more balanced carriers into two individual layers, the B_{c2} in double-side gated bilayer can be varied below and above the B_P (blue squares).

and the localized spin texture in the individual layers is suppressed due to the symmetric doping. Applying a stronger gate accesses a higher T_{c0} and enhances the carrier confinement to the individual layer[17]. This, consequently, weakens the coupling between layers and reveals the hidden local spin polarization in each layer with broken local inversion symmetry[11]. The even higher doping and penetration of the electric field eventually smear out the confined carrier distribution, which also restores the three-dimensional-like behaviour of B_{c2}. This saturated screening effect at strong gating has been observed previously in many ionic liquid gated systems[4,18,23] and is consistent with the stronger localization effect shown in Fig. 2a—the increase of R_N for states with higher T_{c0}—observed at higher gating due to the saturation of screening from both layers.

Single-band pairing at the *K* and *K'* pockets

As shown in Fig. 2b, the carrier concentration required for the onset of the superconducting dome of the double-side gated bilayer is much higher than that of the single-side gating, which can be well understood by the additional *Q*/*Q'* pockets to be filled by the gate induced carriers. Due to the presence of multiple pockets, it is possible to form two different superconducting gaps at both *K* and *Q* points that might have different temperature dependences of B_{c2}, causing the upturn observed in Fig. 4a,b. To remove this concern, we map the differential resistance d*V*/d*I* extracted from a set of *V*–*I* (Supplementary Fig. 4a) measurements at different temperatures for the state with $T_{c0} = 6.63$ K (Fig. 4a). The temperature dependence of critical current density j_c was evaluated from Fig. 4a using 50% of $(dV/dI)_N$ criteria, which approaches 2.84 MA cm^{-2} towards the zero-temperature limit. The best fit of $j_c(T)$ was obtained with the single-band self-field model[24], where the superconducting energy gap Δ_0 and London penetration depth λ_0 were adjustable parameters (Fig. 4b). As shown in Fig. 4b, the gap ratio is obtained by fitting the temperature dependence of j_c. The ratio $\frac{2\Delta_0}{k_B T_{c0}} = 4.49$ is close to the standard Bardeen–Cooper–Schrieffer weak electron–phonon coupling limit favouring the conventional *s*-wave superconductivity[25]. This is consistent with the present understanding of the single-band pairing at *K* and *K'* points, which also eliminates the concern that the upturn observed in the temperature dependence of B_{c2} might be caused by the multiband contribution.

Conclusions

Bilayer 2H-type TMDs are predicted to support a FFLO state[7,8]. In particular, bilayer MoS_2 as a centrosymmetric crystal with broken local inversion symmetry possesses strong alternating Ising SOC and sufficient Josephson coupling to allow for vortex formation between the two layers hosting Ising superconductivity. However, the present bilayer is still in the dirty limit: $l \ll \xi_0$, where $l = v_F\tau$ is the mean free path, v_F is the Fermi velocity, τ is the total scattering time and ξ_0 is the in-plane coherence length. For example, the state with $T_{c0} = 6.63$ K has $l \approx 1.3$ nm and $\xi_0 = 13.6$ nm, respectively. Furthermore, while still being influenced by the orbital depairing mechanism, a bulk doped single crystal of $Ba_3Nb_5S_{13}$ (ref. [26]) has shown mobility of 10^3 cm^2 V^{-1}s^{-1}, which is an essential ingredient for the FFLO state. These findings show that TMDs are promising and flexible candidates to fulfil the stringent theoretical requirements for achieving finite momentum *q* pairing.

Figure 5a compares the effect of Josephson coupling for the superconducting states induced in the conduction bands of TMDs. From B_{c2}/B_P of ~40 as extrapolated from monolayer WS_2, the present control of interlayer coupling (dark blue and red squares

in Fig. 5a) provides an effective way to tune and suppress the Ising protection below B_P. We also compared the variation of B_{c2}/B_P in Fig. 5b for superconductors well known for SOC-induced strong spin protection[27–30], as a function of thickness from monolayer, few-layer, to bulk. The 2H-TaS_2 (purple open circle) and $NbSe_2$ (yellow diamond) are the archetypal examples of intrinsic Ising superconductors. In the bilayer case, the intrinsic spin–orbit and interlayer interactions are competing, therefore, the spin protection in pairing becomes thickness dependent. Comparing with the bilayer 2H-type TaS_2 and $NbSe_2$, the double-side gated bilayer 2H-MoS_2 is a unique platform where these parameters are similar in energy scale and gate controllable. Hence, as a function of gating, both Ising protected (decoupled) and interlayer Josephson dominated (coupled) regimes can be continuously accessed (Sample A, dark blue squares). The ratios of B_{c2}/B_P of bilayer MoS_2 are mostly located near the Pauli limit approaching the bulk intercalated three-dimensional cases at low gating (light green squares). In contrast, B_{c2} of superconductivity induced in a few-layer MoS_2 (open green squares) by single-side gating is mostly determined by β_{SO} and $\alpha_R k_F$, where the competing Rashba SOC is overwhelmed by the strong intrinsic SOC. Especially at low gating, the state is well separated from the bulk showing B_{c2}/B_P of ~6 (ref. [1]). The large gap between these two distinct cases can be bridged by introducing gate tuneable Josephson interaction $\hbar J$ as shown in highly doped single-side gated bilayer MoS_2 (Sample B, red squares). With the effective control of pairing protection by SOC demonstrated above, this all-around gate control of carriers introduces an extra variable degree of freedom for in situ tuning of the spin protection in superconductors.

Online content

Any methods, additional references, Nature Research reporting summaries, source data, statements of code and data availability and associated accession codes are available at https://doi.org/10.1038/s41565-019-0564-1.

Received: 9 May 2019; Accepted: 26 September 2019;
Published online: 4 November 2019

References

1. Lu, J. M. et al. Evidence for two-dimensional Ising superconductivity in gated MoS_2. *Science* **350**, 1353–1357 (2015).
2. Xi, X. et al. Ising pairing in superconducting $NbSe_2$ atomic layers. *Nat. Phys.* **12**, 139–143 (2015).
3. Saito, Y. et al. Superconductivity protected by spin–valley locking in ion-gated MoS_2. *Nat. Phys.* **12**, 144–149 (2015).
4. Lu, J. et al. Full superconducting dome of strong Ising protection in gated monolayer WS_2. *Proc. Natl Acad. Sci. USA* **115**, 3551–3556 (2018).
5. de la Barrera, S. C. et al. Tuning Ising superconductivity with layer and spin–orbit coupling in two-dimensional transition-metal dichalcogenides. *Nat. Commun.* **9**, 1427 (2018).
6. Nakosai, S., Tanaka, Y. & Nagaosa, N. Topological superconductivity in bilayer Rashba system. *Phys. Rev. Lett.* **108**, 147003 (2012).
7. Liu, C.-X. Unconventional superconductivity in bilayer transition metal dichalcogenides. *Phys. Rev. Lett.* **118**, 087001 (2017).
8. Nakamura, Y. & Yanase, Y. Odd-parity superconductivity in bilayer transition metal dichalcogenides. *Phys. Rev. B.* **96**, 054501 (2017).
9. Mizukami, Y. et al. Extremely strong-coupling superconductivity in artificial two-dimensional Kondo lattices. *Nat. Phys.* **7**, 849–853 (2011).
10. Liu, Y. et al. Interface-induced zeeman-protected superconductivity in ultrathin crystalline lead films. *Phys. Rev. X* **8**, 021002 (2018).
11. Zhang, X., Liu, Q., Luo, J.-W., Freeman, A. J. & Zunger, A. Hidden spin polarization in inversion-symmetric bulk crystals. *Nat. Phys.* **10**, 387–393 (2014).
12. Tombros, N. et al. Large yield production of high mobility freely suspended graphene electronic devices on a polydimethylglutarimide based organic polymer. *J. Appl. Phys.* **109**, 093702 (2011).
13. Wang, F. et al. Ionic liquid gating of suspended MoS_2 field-effect transistor devices. *Nano Lett.* **15**, 5284–5288 (2015).
14. Ye, J. T. et al. Superconducting dome in a gate-tuned band insulator. *Science* **338**, 1193–1196 (2012).
15. Eknapakul, T. et al. Electronic structure of a Quasi-freestanding MoS_2 monolayer. *Nano Lett.* **14**, 1312–1316 (2014).
16. Kim, B. S., Rhim, J.-W., Kim, B., Kim, C. & Park, S. R. Determination of the band parameters of bulk 2H-MX_2 (M = Mo, W; X = S, Se) by angle-resolved photoemission spectroscopy. *Sci. Rep.* **6**, 36389 (2016).
17. Brumme, T., Calandra, M. & Mauri, F. First-principles theory of field-effect doping in transition-metal dichalcogenides: Structural properties, electronic structure, Hall coefficient, and electrical conductivity. *Phys. Rev. B.* **91**, 155436 (2015).
18. Ovchinnikov, D. et al. Disorder engineering and conductivity dome in ReS_2 with electrolyte gating. *Nat. Commun.* **7**, 12391 (2016).
19. Coleman, R. V., Eiserman, G. K., Hillenius, S. J., Mitchell, A. T. & Vicent, J. L. Dimensional crossover in the superconducting intercalated layer compound 2H-TaS_2. *Phys. Rev. B.* **27**, 125–139 (1983).
20. Yang, Y. et al. Enhanced superconductivity upon weakening of charge density wave transport in 2H-TaS_2 in the two-dimensional limit. *Phys. Rev. B.* **98**, 035203 (2018).
21. Klemm, R. A., Luther, A. & Beasley, M. R. Theory of the upper critical field in layered superconductors. *Phys. Rev. B.* **12**, 877–891 (1975).
22. Klemm, R. A. *Layered Superconductors Volume 1* International Series of Monographs on Physics, Vol. 153 (Oxford Univ. Press, 2011).
23. Xia, Y., Xie, W., Ruden, P. P. & Frisbie, C. D. Carrier localization on surfaces of organic semiconductors gated with electrolytes. *Phys. Rev. Lett.* **105**, 036802 (2010).
24. Talantsev, E. F. et al. On the origin of critical temperature enhancement in atomically thin superconductors. *2D Mater.* **4**, 025072 (2017).
25. Inosov, D. S. et al. Crossover from weak to strong pairing in unconventional superconductors. *Phys. Rev. B.* **83**, 214520 (2011).
26. Devarakonda, A. et al. Evidence for clean 2D superconductivity and field-induced finite-momentum pairing in a bulk vdW superlattice. Preprint at https://arxiv.org/abs/1906.02065 (2019).
27. Ma, Y. et al. Unusual evolution of B_{c2} and T_c with inclined fields in restacked TaS_2 nanosheets. *NPJ Quantum Mater.* **3**, 34 (2018).
28. Goh, S. K. et al. Anomalous upper critical field in $CeCoIn_5$/$YbCoIn_5$ superlattices with a Rashba-type heavy Fermion interface. *Phys. Rev. Lett.* **109**, 157006 (2012).
29. Sekihara, T., Masutomi, R. & Okamoto, T. Two-dimensional superconducting state of monolayer Pb films grown on GaAs(110) in a strong parallel magnetic field. *Phys. Rev. Lett.* **111**, 057005 (2013).
30. Woollam, J. A. & Somoano, R. B. Superconducting critical fields of alkali and alkaline-earth intercalates of MoS_2. *Phys. Rev. B.* **13**, 3843–3853 (1976).

Methods

Sample fabrication. The MoS_2 flakes were exfoliated using scotch tape from a bulk 2H-MoS_2 single crystal (SPI Supplies). The substrate is prepared by coating lift-off resist and silicon dioxide (LOR/SiO_2) layers ($540 \pm 10/30$ nm) on a degenerately doped Si wafer. Standard electron-beam lithography was used to define electrodes in Hall-bar geometry followed by electron-beam evaporation of Ti/Au (0.5/50 nm). After lift-off in hot *o*-xylene at 80 °C, a second electon-beam lithography step was used to define the undercut structure. Thereafter, the exposed LOR was developed with ethyllactate for the undercut pattern. The suspended bilayer is then immersed into a droplet of a widely used ionic liquid *N*,*N*-diethyl-*N*-(2-methoxyethyl)-*N*-methylammonium bis-(trifluoromethylsulfonyl)-imide (DEME–TFSI).

Transport measurements. The transport measurement was performed using the standard alternating current lock-in technique (Stanford Research SR830 at 13 Hz) in the four-probe configuration. The Keithley K2450 and K182 were used for the DC current excitation and a voltage meter in DC critical current measurements. The sample was gated at 220 K up to 5 V (maximum gate voltage used for this device) of the liquid gate to accumulate the maximum number of carriers and then cooled down below glass transition temperature $T_g \approx 190$ K of ionic liquid at 3 K per min to freeze the ionic motion. All electronic properties were measured at a temperature well below T_g. The different states with different carrier densities were prepared by the thermal release of liquid gate[4], which prepare all states with lower carrier doping.

Data availability

The data that support the plots within this paper and other findings of this study are available from the corresponding author upon reasonable request.

Acknowledgements

J.T.Y. acknowledges funding from the European Research Council (consolidator grant no. 648855, Ig-QPD). We acknowledge D.-H. Xu for a fruitful discussion on the KLB model.

Author contributions

O.Z., J.M.L. and J.T.Y. designed the experiment. O.Z. and J.M.L. fabricated the device and performed the measurements. O.Z., J.M.L., Q.H.C., A.A.E.Y., S.G. and J.T.Y analysed and discussed the data. O.Z. and J.T.Y. wrote the manuscript.

Competing interests

The authors declare no competing interests.

Additional information

Supplementary information is available for this paper at https://doi.org/10.1038/s41565-019-0564-1.

Correspondence and requests for materials should be addressed to J.T.Y.

Reprints and permissions information is available at www.nature.com/reprints.